

Recovery Guarantees for Compressible Signals with Adversarial Noise

Jasjeet Dhaliwal^{1,2} Kyle Hambrook²
 jasjeet_dhaliwal@symantec.com kyle.hambrook@sjsu.edu

¹Center for Advanced Machine Learning, Symantec

²Department of Mathematics and Statistics, San Jose State University

1 Abstract

We provide recovery guarantees for compressible signals that have been corrupted with noise and extend the framework introduced in [1] to defend neural networks against ℓ_0 -norm, ℓ_2 -norm, and ℓ_∞ -norm attacks. Our results are general as they can be applied to most unitary transforms used in practice and hold for ℓ_0 -norm, ℓ_2 -norm, and ℓ_∞ -norm bounded noise. In the case of ℓ_0 -norm noise, we prove recovery guarantees for Iterative Hard Thresholding (IHT) and Basis Pursuit (BP). For ℓ_2 -norm bounded noise, we provide recovery guarantees for BP and for the case of ℓ_∞ -norm bounded noise, we provide recovery guarantees for Dantzig Selector (DS). These guarantees theoretically bolster the defense framework introduced in [1] for defending neural networks against adversarial inputs. Finally, we experimentally demonstrate the effectiveness of this defense framework against an array of ℓ_0 , ℓ_2 and ℓ_∞ norm attacks.

2 Introduction

Signal measurements are often corrupted due to measurement errors and can even be corrupted due to adversarial noise injection. Supposing some structure on the measurement mechanism, is it possible for us to retrieve the original signal from a corrupted measurement? Indeed, it is generally possible to do so using the theory of Compressive Sensing [3] if certain constraints on the measurement mechanism and the signal hold. In order to make the question more concrete, let us consider the class of machine learning problems where the inputs are compressible (i.e., approximately sparse) in some domain. For instance, images and audio signals are known to be compressible in their frequency domain and machine learning algorithms have been shown to perform exceedingly well on classification tasks that take such signals as input [12, 24]. However, it was found in [26] that neural networks can be easily forced into making incorrect predictions by adding adversarial perturbations to their inputs; see also [25, 9, 20, 4]. Further, the adversarial perturbations that led to incorrect predictions were shown to be very small (in either ℓ_0 -norm, ℓ_2 -norm, or ℓ_∞ -norm) and often imperceptible to human beings. For this class of machine learning tasks, we show that it is possible to approximately recover original inputs from adversarial inputs and defend the neural network.

In this paper, we first provide recovery guarantees for compressible signals that have been corrupted by noise bounded in either ℓ_0 -norm, ℓ_2 -norm, or ℓ_∞ -norm. Then we extend the framework

introduced in [1] to defend neural networks against ℓ_0 -norm, ℓ_2 -norm and ℓ_∞ -norm attacks. In the case of ℓ_0 -norm attacks on neural networks, the adversary can perturb a bounded number of elements in the input but has no restriction on how much each element is perturbed in absolute value. In the case of ℓ_2 -norm attacks, the adversary can perturb as many elements as they choose as long as the ℓ_2 -norm of the perturbation vector is bounded. Finally, in the case ℓ_∞ -norm attacks, the adversary is only constrained by the amount of noise added to each pixel. Our recovery guarantees cover all three cases and provide a partial theoretical explanation for the robustness of the defense framework against adversarial inputs. Our contributions can be summarized as follows:

1. We provide recovery guarantees for IHT and BP when the noise budget is bounded in ℓ_0 -norm.
2. We provide recovery guarantees for BP when the noise budget is bounded in the ℓ_2 -norm.
3. We provide recovery guarantees for DS when the noise budget is bounded in the ℓ_∞ -norm and also introduce an additional constraint that improves reconstruction quality.
4. We extend the framework introduced in [1] to defend neural networks against ℓ_0 -norm, ℓ_2 -norm and ℓ_∞ -norm bounded attacks.

The paper is organized as follows. We present the defense framework introduced in [1], which we call Compressive Recovery Defense (CRD), in Section 3.1. We present our main theoretical results (i.e. the recovery guarantees) in Section 3.2 and compare these results to related work in Section 3.3. We establish the Restricted Isometry Property (RIP) in Section 4 provide the proofs of our main results in Sections 5, 6, and 7. We show that CRD can be used to defend against ℓ_0 -norm, ℓ_2 -norm, and ℓ_∞ -norm bounded attacks in Section 8 and conclude the paper in Section 9.

Notation

Let x be a vector in \mathbb{C}^N and let $S \subseteq \{1, \dots, N\}$ with $\bar{S} = \{1, \dots, N\} \setminus S$. We denote by $|S|$, the cardinality of S , i.e. $\text{card}(S)$. The support of x , denoted by $\text{supp}(x)$, is the set of indices of the non-zero entries of x , that is, $\text{supp}(x) = \{i \in \{1, \dots, N\} : x_i \neq 0\}$. The ℓ_0 -quasinorm of x , denoted $\|x\|_0$, is defined to be the number of non-zero entries of x , i.e. $\|x\|_0 = \text{card}(\text{supp}(x))$. We say that x is k -sparse if $\|x\|_0 \leq k$. We denote by x_S either the sub-vector in \mathbb{C}^S consisting of the entries indexed by S or the vector in \mathbb{C}^N that is formed by starting with x and setting the entries indexed by \bar{S} to zero. For example, if $x = [4, 5, -9, 1]$ and $S = \{1, 3\}$, then x_S is either $[4, -9]$ or $[4, 0, -9, 0]$. In the latter case, note $x_{\bar{S}} = x - x_S$. It will always be clear from context, which meaning is intended. If $A \in \mathbb{C}^{m \times N}$ is a matrix, we denote by $A_S \in \mathbb{C}^{m \times |S|}$ the column sub-matrix of A consisting of the columns indexed by S .

We use $x_{h(k)}$ to denote a k -sparse vector in \mathbb{C}^N consisting of the k largest (in absolute value) entries of x with all other entries zero. For example, if $x = [4, 5, -9, 1]$ then $x_{h(2)} = [0, 5, -9, 0]$. Note that $x_{h(k)}$ may not be uniquely defined. In contexts where a unique meaning for $x_{h(k)}$ is needed, we can choose $x_{h(k)}$ out of all possible candidates according to a predefined rule (such as the lexicographic order). We also define $x_{t(k)} = x - x_{h(k)}$.

Let $x = [x_1 \ x_2]^T \in \mathbb{C}^{2n}$ with $x_1, x_2 \in \mathbb{C}^n$, then x is called (k, t) -sparse if x_1 is k -sparse and x_2 is t -sparse. We define $x_{h(k,t)} = [x_{1_{h(k)}} \ x_{2_{h(t)}}]^T$, which is a (k, t) -sparse vector in \mathbb{C}^{2n} . Again, $x_{h(k,t)}$ may not be uniquely defined, but when a unique meaning for $x_{h(k,t)}$ is needed (such as in Algorithm 1), we can choose $x_{h(k,t)}$ out of all possible candidates according to a predefined rule.

3 Main Results

In this section we outline the problem and the framework introduced in [1], state our main theorems, and compare our results to related work.

3.1 Compressive Recovery Defense (CRD)

Consider an image classification problem where $x \in \mathbb{C}^n$ is the image vector (we can assume the image is of size $\sqrt{n} \times \sqrt{n}$ for instance). Then, letting $F \in \mathbb{C}^{n \times n}$ be the unitary Discrete Fourier Transform (DFT) matrix, we get the Fourier coefficients of x as $\hat{x} = Fx$.

It is well known that natural images are approximately sparse in the frequency domain and therefore we can assume that \hat{x} is k -sparse, that is $\|\hat{x}\|_0 \leq k$. In our example of the image classification problem, this means that our machine learning classifier can accept as input the image reconstructed from $\hat{x}_{h(k)}$, and still output the correct decision. That is, the machine learning classifier can accept $F^* \hat{x}_{h(k)}$ as input and still output the correct decision. Now, suppose an adversary perturbs the original image x with a noise vector e , such that we observe $y = x + e$. Noting that y can also be written as $y = F^* \hat{x} + e$, we are interested in recovering an approximation $x^\#$ to $\hat{x}_{h(k)}$, such that when we feed $F^* x^\#$ as input to the classifier, it can still output the correct classification decision.

More generally, this basic framework can be used for adversarial inputs $u = v + d$, where v is the original input and d is the added noise vector, as long as there exists a matrix A such that $u = A\hat{v} + d$, where \hat{v} is approximately sparse and $\|d\|_p \leq \eta$ for some $p, \eta \geq 0$. If we can recover an approximation $v^\#$ to \hat{v} with bounds on the recovery error, then we can use $v^\#$ to reconstruct an approximation $Av^\#$ to v with controlled error.

This general framework was proposed by [1]. Moving forward, we refer to this general framework as Compressive Recovery Defense (CRD) and utilize it to defend neural networks against ℓ_0 , ℓ_2 , and ℓ_∞ -norm attacks. As observed in [1], $x^{[0]}$ in Algorithm 1, can be initialized randomly to defend against a reverse-engineering attack. In the case of Algorithm 2, the minimization problem can be posed as a Second Order Cone Programming (SOCP) problem and it appears non-trivial to create a reverse engineering attack that will retain the adversarial noise through the recovery and reconstruction process. The same reasoning holds for Algorithm 3 which can be posed as a Linear Programming (LP) problem.

3.2 Results

Theorem 1 (ℓ_0 -norm IHT). *Let $A = [F \ I] \in \mathbb{C}^{n \times 2n}$, where $F \in \mathbb{C}^{n \times n}$ is a unitary matrix with $|F_{ij}|^2 \leq \frac{c}{n}$ and $I \in \mathbb{C}^{n \times n}$ is the identity matrix. Let $y = F\hat{x} + e$, where $\hat{x}, e \in \mathbb{C}^n$, and e is t -sparse. Let $1 \leq k \leq n$ be integer and let $x^{[T+1]} = \text{IHT}(y, A, k, t, T)$ where $x^{[T+1]} = [\hat{x}^{[T+1]} \ e^{[T+1]}]^T \in \mathbb{C}^{2n}$ with $\hat{x}^{[T+1]}, e^{[T+1]} \in \mathbb{C}^n$.*

Define $\rho := \sqrt{27} \sqrt{\frac{ckt}{n}}$, $\tau(1 - \rho) := \sqrt{3} \sqrt{1 + 2\sqrt{\frac{ckt}{n}}}$. If $0 < \rho < 1$, then:

$$\|\hat{x}^{[T+1]} - \hat{x}_{h(k)}\|_2 \leq \rho^{(T+1)} \sqrt{\|\hat{x}_{h(k)}\|_2^2 + \|e\|_2^2} + \tau \|\hat{x}_{t(k)}\|_2 \quad (1)$$

Moreover for any $0 < \epsilon < 1$ and any $T \geq \left(\frac{\log(1/\epsilon) + \log(\sqrt{\|\hat{x}_{h(k)}\|_2^2 + \|e\|_2^2})}{\log(1/\rho)} \right)$, we get:

$$\|\hat{x}^{[T+1]} - \hat{x}_{h(k)}\|_2 \leq \tau \|\hat{x}_{t(k)}\|_2 + \epsilon \quad (2)$$

Now define $\rho := 2\sqrt{2}\sqrt{\frac{ckt}{n}}$, $\tau(1 - \rho) := 2$. If $0 < \rho < 1$, then:

$$\|\hat{x}^{[T+1]} - \hat{x}_{h(k)}\|_2 \leq \rho^{(T+1)} \|\hat{x}_{h(k)}\|_2 + \tau(\|\hat{x}_{t(k)}\|_2 + \|e\|_2) \quad (3)$$

Moreover for any $0 < \epsilon < 1$ and any $T \geq \left(\frac{\log(1/\epsilon) + \log(\|\hat{x}_{h(k)}\|_2)}{\log(1/\rho)}\right)$, we get:

$$\|\hat{x}^{[T+1]} - \hat{x}_{h(k)}\|_2 \leq \tau(\|\hat{x}_{t(k)}\|_2 + \|e\|_2) + \epsilon \quad (4)$$

Note that for practical applications, (3) and (4) provide error bounds for larger values of k and t than (1) and (2), at the expense of the extra error term $\|e\|_2$. Further, the above results apply to unitary transformations such as the Fourier Transform, Cosine Transform, Sine Transform, Hadamard Transform, and other wavelet transforms. Next, we consider the recovery error for ℓ_0 -norm bounded noise with BP instead of IHT. Providing bounds for BP is useful as there are cases¹ when BP provides recovery guarantees against a larger ℓ_0 noise budget than IHT. We note that since Algorithm 2 is not adapted to the structure of the matrix A in the statement of Theorem 2, one can expect the guarantees to be weaker.

Theorem 2 (ℓ_0 -norm BP). *Let $A = [F \ I] \in \mathbb{C}^{n \times 2n}$, where $F \in \mathbb{C}^{n \times n}$ is a unitary matrix with $|F_{ij}|^2 \leq \frac{c}{n}$ and $I \in \mathbb{C}^{n \times n}$ is the identity matrix. Let $y = F\hat{x} + e$, and let $1 \leq k, t \leq n$ be integers. Define*

$$\delta_{k,t} = \sqrt{\frac{ckt}{n}}, \quad \beta = \sqrt{\frac{\max\{k, t\}c}{n}}, \quad \theta = \frac{\sqrt{k+t}}{(1 - \delta_{k,t})}\beta, \quad \tau = \frac{\sqrt{1 + \delta_{k,t}}}{1 - \delta_{k,t}}$$

If $0 < \delta_{k,t} < 1$ and $0 < \theta < 1$, then for a solution $x^\# = BP(y, A, \|\hat{x}_{t(k)}\|_2)$ of Algorithm 2, we have the error bound

$$\|\hat{x}^\# - \hat{x}_{h(k)}\|_2 \leq \left(\frac{2\tau\sqrt{k+t}}{1 - \theta} \left(1 + \frac{\beta}{1 - \delta_{k,t}}\right) + 2\tau\right) \|\hat{x}_{t(k)}\|_2 \quad (5)$$

where we write $x^\# = [\hat{x}^\# \ e^\#]^T \in \mathbb{C}^{2n}$ with $\hat{x}^\#, e^\# \in \mathbb{C}^n$.

Our third result covers the case when the noise is bounded in ℓ_2 -norm. Note that the result covers all unitary matrices and removes the restriction on the magnitude of their elements.

Theorem 3 (ℓ_2 -norm BP). *Let $F \in \mathbb{C}^{n \times n}$ be a unitary matrix and let $y = F\hat{x} + e$, where $\hat{x} \in \mathbb{C}^n$ is k -sparse and $e \in \mathbb{C}^n$. If $\|e\|_2 \leq \eta$, then for a solution $x^\# = BP(y, F, \eta)$ of Algorithm 2, we have the error bound*

$$\|x^\# - \hat{x}\|_1 \leq 4\sqrt{k}\eta \quad (6)$$

$$\|x^\# - \hat{x}\|_2 \leq 6\eta \quad (7)$$

Finally, we provide recovery guarantees when the noise is bounded in ℓ_∞ -norm.

Theorem 4 (ℓ_∞ -norm DS). *Let $F \in \mathbb{C}^{n \times n}$ be a unitary matrix and let $y = F\hat{x} + e$, where $\hat{x} \in \mathbb{C}^n$ is k -sparse and $e \in \mathbb{C}^n$. If $\|e\|_\infty \leq \eta_1$ and $\|F^*e\|_\infty \leq \eta_2$, then for a solution $x^\# = DS(y, F, \eta_1, \eta_2)$ of Algorithm 3, we have the error bound*

$$\|x^\# - \hat{x}\|_1 \leq 4k\eta_2 \quad (8)$$

$$\|x^\# - \hat{x}\|_2 \leq 6\sqrt{k}\eta_2 \quad (9)$$

¹ As shown in Section 8.1.1 and Section 8.2.2

3.3 Comparison to Related Work

The authors of [1] introduced the CRD framework which inspired this work. In fact, the main theorem (Theorem 2.2) of [1] also provides an approximation error bound for recovery via IHT. First, we note that the statement of the Theorem 2.2 in [1] is missing the required hypothesis $t = O(n/k)$. This hypothesis appears in Lemma 3.6 of [1], which is used to prove Theorem 2.2 of [1], but it appears to have been accidentally dropped from the statement of Theorem 2.2 of [1]. By making the constants explicit, the proof of Lemma 3.6 of [1] gives the same restricted isometry property that we do in Theorem 7. Therefore, the guarantees of (13) and (14) are essentially the same as those in Theorem 2.2 in [1]. The main difference is that, to derive recovery guarantees for IHT from the restricted isometry property, we utilize Theorem 8 below (which is a modified version of Theorem 6.18 of [8]) while the authors of [1] utilize Theorem 3.4 in [1] (which is taken from [2]). In addition, we also provide recovery error bounds for IHT in (3) and (4) of Theorem 1 that hold for larger values of k and t at the expense of the additional error term $\|e\|_2$.

Other works that provide guarantees include [11] and [5] where the authors frame the problem as one of regularizing the Lipschitz constant of a network and provide a lower bound on the norm of the perturbation required to change the classifier decision. The authors of [22] use robust optimization to perturb the training data and provide a training procedure that updates parameters based on worst case perturbations. A similar approach to [22] is [28] in which the authors use robust optimization to provide lower bounds on the norm of adversarial perturbations on the training data. In [16], the authors use techniques from Differential Privacy [7] in order to augment the training procedure of the classifier to improve robustness to adversarial inputs. Another approach using randomization is [17] in which the authors add i.i.d. Gaussian noise to the input and provide guarantees of maintaining classifier predictions as long as the ℓ_2 -norm of the attack vector is bounded by a function that depends on the output of the classifier.

Most defenses against adversarial inputs do not come with theoretical guarantees. Instead, a large body of research has focused on finding practical ways to improve robustness to adversarial inputs by either augmenting the training data [9], using adversarial inputs from various networks [27], or by reducing the dimensionality of the input [30]. For instance, [18] use robust optimization to make the network robust to worst case adversarial perturbations on the training data. However, the effectiveness of their approach is determined by the amount and quality of training data available and its similarity to the distribution of the test data. An approach similar to ours but without any theoretical guarantees is [21]. In this work, the authors use Generative Adversarial Networks (GANs) to estimate the distribution of the training data and during inference, use a GAN to reconstruct an input that is most similar to a given test input and is not adversarial.

4 Restricted Isometry Property

We now establish the restricted isometry property for certain structured matrices. First, we give some definitions.

Definition 5. Let A be a matrix in $\mathbb{C}^{m \times N}$, let $M \subseteq \mathbb{C}^N$, and let $\delta \geq 0$. We say that A satisfies the M -restricted isometry property (or M-RIP) with constant δ if

$$(1 - \delta)\|x\|_2^2 \leq \|Ax\|_2^2 \leq (1 + \delta)\|x\|_2^2$$

for all $x \in M$.

Definition 6. We define M_k to be the set of all k -sparse vectors in \mathbb{C}^N and similarly define $M_{k,t}$ to be the set of (k, t) -sparse vectors in \mathbb{C}^{2n} . In other words, $M_{k,t}$ is the following subset of \mathbb{C}^{2n} :

$$M_{k,t} = \{x = [x_1 \ x_2]^T \in \mathbb{C}^{2n} : x_1 \in \mathbb{C}^n, x_2 \in \mathbb{C}^n, \|x_1\|_0 \leq k, \|x_2\|_0 \leq t\}$$

We define $S_{k,t}$ to be the following collection of subsets of $\{1, \dots, 2n\}$:

$$S_{k,t} = \{S_1 \cup S_2 : S_1 \subseteq \{1, \dots, n\}, S_2 \subseteq \{n+1, \dots, 2n\}, \text{card}(S_1) \leq k, \text{card}(S_2) \leq t\}$$

Note that $S_{k,t}$ is the collection of supports of vectors in $M_{k,t}$.

Theorem 7. Let $A = [F \ I] \in \mathbb{C}^{n \times 2n}$, where $F \in \mathbb{C}^{n \times n}$ is a unitary matrix with $|F_{ij}|^2 \leq \frac{c}{n}$ and $I \in \mathbb{C}^{n \times n}$ is the identity matrix. Then

$$\left(1 - \sqrt{\frac{ckt}{n}}\right) \|x\|_2^2 \leq \|Ax\|_2^2 \leq \left(1 + \sqrt{\frac{ckt}{n}}\right) \|x\|_2^2 \quad (10)$$

for all $x \in M_{k,t}$. In other words, A satisfies the $M_{k,t}$ -RIP property with constant $\sqrt{\frac{ckt}{n}}$.

Proof. In this proof, if B denotes a matrix in $\mathbb{C}^{n \times n}$, then $\lambda_1(B), \dots, \lambda_n(B)$ denote the eigenvalues of B ordered so that $|\lambda_1(B)| \leq \dots \leq |\lambda_n(B)|$. It suffices to fix an $S = S_1 \cup S_2 \in S_{k,t}$ and prove (10) for all non-zero $x \in \mathbb{C}^S$.

Since $A_S^* A_S$ is normal, there is an orthonormal basis of eigenvectors u_1, \dots, u_{k+t} for $A_S^* A_S$, where u_i corresponds to the eigenvalue $\lambda_i(A_S^* A_S)$. For any non-zero $x \in \mathbb{C}^S$, we have $x = \sum_{i=1}^{k+t} c_i u_i$ for some $c_i \in \mathbb{C}$, so

$$\frac{\|Ax\|_2^2}{\|x\|_2^2} = \frac{\langle A_S^* A_S x, x \rangle}{\langle x, x \rangle} = \frac{\sum_{i=1}^{k+t} \lambda_i(A_S^* A_S) c_i^2}{\sum_{i=1}^{k+t} c_i^2}. \quad (11)$$

Thus it will suffice to prove that $|\lambda_i(A_S^* A_S) - 1| \leq \sqrt{\frac{ckt}{n}}$ for all i . Moreover,

$$|\lambda_i(A_S^* A_S) - 1| = |\lambda_i(A_S^* A_S - I)| = \sqrt{\lambda_i((A_S^* A_S - I)^*(A_S^* A_S - I))} \quad (12)$$

where the last equality holds because $A_S^* A_S - I$ is normal. By combining (11) and (12), we see that (10) will hold upon showing that the eigenvalues of $(A_S^* A_S - I)^*(A_S^* A_S - I)$ are bounded by ckt/n .

So far we have not used the structure of A , but now we must. Observe that $(A_S^* A_S - I)^*(A_S^* A_S - I)$ is a block diagonal matrix with two diagonal blocks of the form $X^* X$ and XX^* . Therefore the three matrices $(A_S^* A_S - I)^*(A_S^* A_S - I)$, $X^* X$, and XX^* have the same non-zero eigenvalues. Moreover, X is simply the matrix F_{S_1} with those rows not indexed by S_2 deleted. The hypotheses on F imply that the entries of $X^* X$ satisfy $|(X^* X)_{ij}| \leq \frac{ct}{n}$. So the Gershgorin disc theorem implies that each eigenvalue λ of $X^* X$ and (hence) of $(A_S^* A_S - I)^*(A_S^* A_S - I)$ satisfies $|\lambda| \leq \frac{ckt}{n}$. \square

5 Iterative Hard Thresholding

First we present Theorem 8 and then use it to prove Theorem 1.

Algorithm 1 (k, t) -Iterative Hard Thresholding

Input: The observed vector $y \in \mathbb{C}^n$, the measurement matrix $A \in \mathbb{C}^{n \times 2n}$, and positive integers $k, t, T \in \mathbb{Z}^+$

Output: $x^{[T+1]} \in M_{k,t}$

```
1: procedure IHT( $y, A, k, t, T$ )
2:    $x^{[0]} \leftarrow 0$ 
3:   for  $i \in [0, \dots, T]$  do
4:      $z^{[i+1]} \leftarrow x^{[i]} + A^*(y - Ax^{[i]})$ 
5:      $x^{[i+1]} = (z^{[i+1]})_{h(k,t)}$ 
6:   return  $x^{[T+1]}$ 
```

Theorem 8. Let $A \in \mathbb{C}^{n \times 2n}$ be a matrix. Let $1 \leq k, t \leq n$ be positive integers and suppose δ_3 is a $M_{3k,3t}$ -RIP constant for A and that δ_2 is a $M_{2k,2t}$ -RIP constant for A . Let $x \in \mathbb{C}^{2n}$, $r \in \mathbb{C}^n$, $y = Ax + r$, and $S \in S_{k,t}$. Letting $x^{[T+1]} = \text{IHT}(y, A, k, t, T)$, if $\delta_3 < 1/\sqrt{3}$, then we have the approximation error bound

$$\|x^{[T+1]} - x_S\|_2 \leq \rho^{(T+1)} \|x^{[0]} - x_S\|_2 + \tau \|Ax_{\bar{S}} + r\|_2$$

where $\rho := \sqrt{3}\delta_3 < 1$ and $(1 - \rho)\tau = \sqrt{3}\sqrt{1 + \delta_2} \leq 2.18$. Thus, the first term on the right goes to 0 as T goes to ∞ .

Theorem 8 is a modification of Theorem 6.18 of [8]. More specifically, Theorem 6.18 of [8] considers M_{3k} , M_{2k} , and S_k in place of $M_{3k,3t}$ and $M_{2k,2t}$ and $S_{k,t}$ and any dimension N in place of $2n$. The proofs are very similar, so we omit the proof of Theorem 8. We will now prove a lemma that will be required for the proof of Theorem 1. For the proof of Lemma 9 and Theorem 1, we use the following convention: let $A \in \mathbb{C}^{m \times N}$ be a matrix, then, we denote by $(A)_S$, the $m \times N$ matrix that is obtained by starting with A and zeroing out the columns indexed by \bar{S} . Note that $(A)_S = A - (A)_{\bar{S}}$.

Lemma 9. Let $F \in \mathbb{C}^{n \times n}$ be a unitary matrix with $|F_{ij}|^2 \leq \frac{c}{n}$ and let $S \subseteq [n]$ be a index set with $|S| = t$. Then for any k -sparse vector $z \in \mathbb{C}^n$, we have:

$$\|(F^*)_S Fz\|_2^2 \leq \frac{ktc}{n} \|z\|_2^2$$

Proof. First note that $(F^*)_S \in \mathbb{C}^{n \times n}$ contains only t non-zero columns since $|S| = t$. Therefore, we have $|((F^*)_S F)_{ij}| \leq \frac{tc}{n}$ since $|F_{ij}|^2 \leq \frac{c}{n}$. Further, since the non-zero columns of $(F^*)_S$ are orthogonal to each other, we get $((F^*)_S)^*(F^*)_S = (I)_S$, where $I \in \mathbb{C}^{n \times n}$ is the identity matrix. Using this, we have for any $w \in \mathbb{C}^n$,

$$\|(F^*)_S Fw\|_2^2 = \langle (F^*)_S Fw, (F^*)_S Fw \rangle = \langle ((F^*)_S F)^* (F^*)_S Fw, w \rangle = \langle (F^*)_S Fw, w \rangle = |\langle (F^*)_S Fw, w \rangle|$$

Now let $V \subseteq [n]$ be any index set with cardinality k , that is $|V| = k$ and let $z \in \mathbb{C}^n$ be any

vector supported on V . We then get,

$$\begin{aligned} \|(F^*)_S F z\|_2^2 &= |((F^*)_S F z, z)| = \left| \sum_{k \in V} z_k^* \left(\sum_{j \in V} ((F^*)_S F)_{kj} z_j \right) \right| \leq \sum_{k \in V} |z_k^*| \left(\sum_{j \in V} |((F^*)_S F)_{kj}| |z_j| \right) \\ &\leq \sum_{k \in V} |z_k^*| \left(\frac{tc}{n} \sum_{j \in V} |z_j| \right) \\ &= \frac{tc}{n} \|z\|_1^2 \leq \frac{ktc}{n} \|z\|_2^2 \end{aligned}$$

where we use the fact that z is k -sparse for the last inequality. \square

Now we provide the proof for Theorem 1.

Proof of Theorem 1. Theorem 7 implies that the statement of Theorem 8 holds with

$\delta_3 = \sqrt{\frac{c \cdot 3k \cdot 3t}{n}}$ and $\delta_2 = \sqrt{\frac{c \cdot 2k \cdot 2t}{n}}$. Noting that $y = A[\hat{x}_{h(k)} \ e]^T + F\hat{x}_{t(k)}$, where $[\hat{x}_{h(k)} \ e]^T \in M_{k,t}$, set $x^{[T+1]} = IHT(y, A, k, t, T)$ and apply Theorem 8 with $x = [\hat{x}_{h(k)} \ e]^T$, $r = F\hat{x}_{t(k)}$, and $S = \text{supp}(x)$. Letting $x^{[T+1]} = [\hat{x}^{[T+1]} \ e^{[T+1]}]^T$, use the facts that $\|\hat{x}^{[T+1]} - \hat{x}_{h(k)}\|_2 \leq \|x^{[T+1]} - x_S\|_2$ and $\|F\hat{x}_{t(k)}\|_2 = \|\hat{x}_{t(k)}\|_2$. That will give (1). Letting $T = \left(\frac{\log(1/\epsilon) + \log(\sqrt{\|\hat{x}_{h(k)}\|_2^2 + \|e\|_2^2})}{\log(1/\rho)} \right)$, gives $\rho^T \sqrt{\|\hat{x}_{h(k)}\|_2^2 + \|e\|_2^2} \leq \epsilon$, which can be substituted in (1) to get (2). Noting that $\|e^{[T]} - e\|_2 \leq \tau \|\hat{x}_{t(k)}\|_2 + \epsilon$, we can use the same reasoning as used in [1] to get:

$$\|\hat{x}^{[T+1]} - \hat{x}_{h(k)}\|_\infty \leq \sqrt{\frac{2ct}{n}} (\tau \|\hat{x}_{t(k)}\|_2 + \epsilon) \quad (13)$$

$$\|\hat{x}^{[T+1]} - \hat{x}_{h(k)}\|_2 \leq \sqrt{\frac{4ckt}{n}} (\tau \|\hat{x}_{t(k)}\|_2 + \epsilon) \quad (14)$$

which are the essentially the same as the results of Theorem 2.2 in [1].

Now we prove (3). Let $z^{[T]}$ be as defined in Algorithm 1 with $z^{[T]} = [z_1^{[T]} \ z_2^{[T]}]^T \in \mathbb{C}^{2n}$ where $z_1^{[T]}, z_2^{[T]} \in \mathbb{C}^n$. Note that $\hat{x}^{[T]} = (z_1^{[T]})_{h(k)}$. Therefore, we have $z_1^{[T]} = F^*(y - e^{[T-1]})$, where $e^{[T-1]} = (y - F\hat{x}^{[T-2]})_{h(t)}$. Now let S be the set of indices selected by the hard thresholding operation $h(t)$ to get $e^{[T-1]}$. Then observe that $z_1^{[T]} = F^*(y - (y - F\hat{x}^{[T-2]})_S)$. Next, note that $\|z_1^{[T]} - \hat{x}^{[T]}\|_2^2 \leq \|z_1^{[T]} - \hat{x}_{h(k)}\|_2^2$ as $\hat{x}^{[T]}$ is a best k -sparse approximation to $z_1^{[T]}$. We can thus write,

$$\|(z_1^{[T]} - \hat{x}_{h(k)}) - (\hat{x}^{[T]} - \hat{x}_{h(k)})\|_2^2 = \|z_1^{[T]} - \hat{x}_{h(k)}\|_2^2 - 2\text{Re}\langle z_1^{[T]} - \hat{x}_{h(k)}, \hat{x}^{[T]} - \hat{x}_{h(k)} \rangle + \|\hat{x}^{[T]} - \hat{x}_{h(k)}\|_2^2$$

Therefore, we have,

$$\begin{aligned} \|\hat{x}^{[T]} - \hat{x}_{h(k)}\|_2^2 &\leq 2\text{Re}\langle z_1^{[T]} - \hat{x}_{h(k)}, \hat{x}^{[T]} - \hat{x}_{h(k)} \rangle \\ &\leq 2|\langle z_1^{[T]} - \hat{x}_{h(k)}, \hat{x}^{[T]} - \hat{x}_{h(k)} \rangle| \\ &\leq 2\|z_1^{[T]} - \hat{x}_{h(k)}\|_2 \|\hat{x}^{[T]} - \hat{x}_{h(k)}\|_2 \end{aligned}$$

If $\|\hat{x}^{[T]} - \hat{x}_{h(k)}\|_2 > 0$, then $\|\hat{x}^{[T]} - \hat{x}_{h(k)}\|_2 \leq 2\|z_1^{[T]} - \hat{x}_{h(k)}\|_2$. Now note that,

$$\begin{aligned} z_1^{[T]} &= \hat{x} + F^*e - F^*(F(\hat{x} - \hat{x}^{[T-2]} + e))_S \\ &= \hat{x} + F^*e - (F^*)_S(F(\hat{x} - \hat{x}^{[T-2]} + e)) \\ &= \hat{x} + (F^* - (F^*)_S)e - (F^*)_SF(\hat{x} - \hat{x}^{[T-2]}) \end{aligned}$$

Using the fact that $(F^*)_{\bar{S}} = F^* - (F^*)_S$, we can simplify the above to get:

$$\|z_1^{[T]} - \hat{x}_{h(k)}\|_2 = \|(F^*)_{\bar{S}}F\hat{x}_{t(k)} + (F^*)_{\bar{S}}e - (F^*)_SF(\hat{x}_{h(k)} - \hat{x}^{[T-2]})\|_2$$

Therefore,

$$\begin{aligned} \|\hat{x}^{[T]} - \hat{x}_{h(k)}\|_2 &\leq 2 \left(\|(F^*)_{\bar{S}}F\|_{2 \rightarrow 2} \|\hat{x}_{t(k)}\|_2 + \|(F^*)_{\bar{S}}\|_{2 \rightarrow 2} \|e\|_2 + \|(F^*)_SF(\hat{x}_{h(k)} - \hat{x}^{[T-2]})\|_2 \right) \\ &\leq 2 (\|\hat{x}_{t(k)}\|_2 + \|e\|_2) + 2 \|(F^*)_SF(\hat{x}_{h(k)} - \hat{x}^{[T-2]})\|_2 \end{aligned}$$

where we use $\|(F^*)_{\bar{S}}\|_{2 \rightarrow 2} \leq \|F^*\|_{2 \rightarrow 2} = 1$. Now since $\hat{x}_{h(k)} - \hat{x}^{[T-2]}$ is $2k$ -sparse, we can use the result of Lemma 9 to get:

$$\|\hat{x}^{[T]} - \hat{x}_{h(k)}\|_2 \leq 2 (\|\hat{x}_{t(k)}\|_2 + \|e\|_2) + 2 \left(\sqrt{\frac{2ktc}{n}} \right) \|\hat{x}^{[T-2]} - \hat{x}_{h(k)}\|_2$$

Now let $\rho = 2\sqrt{2}\sqrt{\frac{ktc}{n}}$, $\tau(1 - \rho) = 2$ and note that if $\rho < 1$, we can use induction on T to get (3). Then for any $0 < \epsilon < 1$ and any $T \geq \left(\frac{\log(1/\epsilon) + \log(\|\hat{x}_{h(k)}\|_2)}{\log(1/\rho)} \right)$, we have $\rho^T(\|\hat{x}_{h(k)}\|_2) \leq \epsilon$ which gives us (4). □

6 Basis Pursuit

Next we introduce the Basis Pursuit algorithm and prove its recovery guarantees for ℓ_0 -norm and ℓ_2 -norm noise. We begin by stating some definitions that will be required in the proofs of the main theorems.

Algorithm 2 Basis Pursuit

Input: The observed vector $y \in \mathbb{C}^m$, where $y = A\hat{x} + e$, the measurement matrix $A \in \mathbb{C}^{m \times N}$, and the norm of the error vector η such that $\|e\|_2 \leq \eta$

Output: $x^\# \in \mathbb{C}^N$

- 1: **procedure** BP(y, A, η)
 - 2: $x^\# \leftarrow \arg \min_{z \in \mathbb{C}^N} \|z\|_1$ subject to $\|Az - y\|_2 \leq \eta$
 - 3: **return** $x^\#$
-

Definition 10. The matrix $A \in \mathbb{C}^{m \times N}$ satisfies the robust null space property with constants $0 < \rho < 1$, $\tau > 0$ and norm $\|\cdot\|$ if for every set $S \subseteq [N]$ with $\text{card}(S) \leq s$ and for every $v \in \mathbb{C}^N$ we have

$$\|v_S\|_1 \leq \rho \|v_{\bar{S}}\|_1 + \tau \|Av\|$$

Definition 11. The matrix $A \in \mathbb{C}^{m \times N}$ satisfies the ℓ_q robust null space property of order s with constants $0 < \rho < 1$, $\tau > 0$ and norm $\|\cdot\|$ if for every set $S \subseteq [N]$ with $\text{card}(S) \leq s$ and for every $v \in \mathbb{C}^N$ we have

$$\|v_S\|_q \leq \frac{1}{s^{1-1/q}} \rho \|v_{\bar{S}}\|_1 + \tau \|Av\|$$

Note that if $q = 1$ then this is simply the robust null space property.

The proof of Theorem 2 requires the following theorem (whose full proof is given in the [8]).

Theorem 12 (Theorem 4.33 in [8]). *Let a_1, \dots, a_N be the columns of $A \in \mathbb{C}^{m \times N}$, let $x \in \mathbb{C}^N$ with s largest absolute entries supported on S , and let $y = Ax + e$ with $\|e\|_2 \leq \eta$. For $\delta, \beta, \gamma, \theta, \tau \geq 0$ with $\delta < 1$, assume that:*

$$\|A_S^* A_S - I\|_{2 \rightarrow 2} \leq \delta, \quad \max_{l \in \bar{S}} \|A_S^* a_l\|_2 \leq \beta,$$

and that there exists a vector $u = A^* h \in \mathbb{C}^N$ with $h \in \mathbb{C}^m$ such that

$$\|u_S - \text{sgn}(x_S)\|_2 \leq \gamma, \quad \|u_{\bar{S}}\|_\infty \leq \theta, \quad \text{and } \|h\|_2 \leq \tau \sqrt{s}.$$

If $\rho := \theta + \frac{\beta\gamma}{(1-\delta)} < 1$, then a minimizer $x^\#$ of $\|z\|_1$ subject to $\|Az - y\|_2 \leq \eta$ satisfies:

$$\|x^\# - x\|_2 \leq \frac{2}{(1-\rho)} \left(1 + \frac{\beta}{(1-\delta)}\right) \|x_{\bar{S}}\|_1 + \left(\frac{2(\mu\gamma + \tau\sqrt{s})}{1-\rho} \left(1 + \frac{\beta}{1-\delta}\right) + 2\mu\right) \eta$$

$$\text{where } \mu := \frac{\sqrt{1+\delta}}{1-\delta} \text{ and } \text{sgn}(x)_i = \begin{cases} 0, & x_i = 0 \\ 1, & x_i > 0. \\ -1, & x_i < 0 \end{cases}$$

Lemma 13. *Let $A \in \mathbb{C}^{n \times 2n}$, if $\|Ax\|_2^2 \leq (1+\delta)\|x\|_2^2$ for all $x \in M_{k,t}$, then, $\|A_S^* A_S - I\|_{2 \rightarrow 2} \leq \delta$, for any $S \in S_{k,t}$.*

Proof. Let $S \in S_{k,t}$ be given. Then for any $x \in \mathbb{C}^S$, we have

$$\|A_S x\|_2^2 - \|x\|_2^2 \leq \delta \|x\|_2^2$$

We can re-write this as : $\|A_S x\|_2^2 - \|x\|_2^2 = \langle A_S x, A_S x \rangle - \langle x, x \rangle = \langle (A_S^* A_S - I)x, x \rangle$. Noting that $A_S^* A_S - I$ is Hermitian, we have:

$$\|A_S^* A_S - I\|_{2 \rightarrow 2} = \max_{x \in \mathbb{C}^S \setminus \{0\}} \frac{\langle (A_S^* A_S - I)x, x \rangle}{\|x\|_2^2} \leq \delta$$

□

Proof of Theorem 2. We will derive (5) by showing that the matrix A satisfies all the hypotheses in Theorem 12 for every vector in $M_{k,t}$.

First note that by Theorem 7, A satisfies the $M_{k,t}$ -RIP property with constant $\delta_{k,t} := \sqrt{\frac{ckt}{n}}$. Therefore, by Lemma 13, for any $S \in S_{k,t}$, we have $\|A_S^* A_S - I\|_{2 \rightarrow 2} \leq \delta_{k,t}$. Since $A_S^* A_S$ is a positive semi-definite matrix, it has only non-negative eigenvalues that lie in the range $[1 - \delta_{k,t}, 1 + \delta_{k,t}]$. Since $\delta_{k,t} < 1$ by assumption, $A_S^* A_S$ is injective. Thus, we can set: $h = A_S (A_S^* A_S)^{-1} \text{sgn}(x_S)$ and get:

$$\|h\|_2 = \|A_S (A_S^* A_S)^{-1} \text{sgn}(x_S)\|_2 \leq \|A_S\|_{2 \rightarrow 2} \|(A_S^* A_S)^{-1}\|_{2 \rightarrow 2} \|\text{sgn}(x_S)\|_2 \leq \tau \sqrt{k+t}$$

where $\tau = \frac{\sqrt{1+\delta_{k,t}}}{1-\delta_{k,t}}$ and we have used the following facts: since $\|A_S^* A_S - I\|_{2 \rightarrow 2} \leq \delta_{k,t} < 1$, we get that $\|(A_S^* A_S)^{-1}\|_{2 \rightarrow 2} \leq \frac{1}{1-\delta_{k,t}}$ and that the largest singular value of A_S is less than $\sqrt{1+\delta_{k,t}}$. Now let $u = A^* h$, then $\|u_S - \text{sgn}(x_S)\|_2 = 0$. Now we need to bound the value $\|u_{\bar{S}}\|_\infty$. Denoting row j of $A_S^* A_S$ by the vector v_j , we see that it has at most $\max\{k, t\}$ non-zero entries and that $|(v_j)_l|^2 \leq \frac{c}{n}$ for $l = 1, \dots, (k+t)$. Therefore, for any element $(u_{\bar{S}})_j$, we have:

$$|(u_{\bar{S}})_j| = |\langle (A_S^* A_S)^{-1} \text{sgn}(x_S), (v_j)^* \rangle| \leq \|(A_S^* A_S)^{-1}\|_{2 \rightarrow 2} \|\text{sgn}(x_S)\|_2 \|v_j\|_2 \leq \frac{\sqrt{k+t}}{1-\delta_{k,t}} \sqrt{\frac{\max\{k, t\}c}{n}}$$

Defining $\beta := \sqrt{\frac{\max\{k, t\}c}{n}}$ and $\theta := \frac{\sqrt{k+t}}{1-\delta_{k,t}}\beta$, we get $\|u_{\bar{S}}\|_\infty \leq \theta < 1$ and also observe that $\max_{l \in \bar{S}} \|A_S^* a_l\|_2 \leq \beta$. Therefore, all the hypotheses of Theorem 12 have been satisfied. Note that $y = F\hat{x} + e = A[\hat{x}_{h(k)} \ e]^T + F\hat{x}_{t(k)}$, Therefore, setting $x^\# = \text{BP}(y, A, \|\hat{x}_{t(k)}\|_2)$, we use the fact $\|F\hat{x}_{t(k)}\|_2 = \|\hat{x}_{t(k)}\|_2$ combined with the bound in Theorem 12 to get (5):

$$\|\hat{x}^\# - \hat{x}_{h(k)}\|_2 \leq \left(\frac{2\tau\sqrt{k+t}}{1-\theta} \left(1 + \frac{\beta}{1-\delta_{k,t}} \right) + 2\tau \right) \|\hat{x}_{t(k)}\|_2$$

where we write $x^\# = [\hat{x}^\# \ e^\#]^T$ with $\hat{x}^\#, e^\# \in \mathbb{C}^n$. \square

We now focus on proving Theorem 3. In order to do so, we will need some lemmas that will be used in the main proof.

Lemma 14. *If a matrix $A \in \mathbb{C}^{m \times N}$ satisfies the ℓ_2 robust null space property for $S \subset [N]$, with $\text{card}(S) = s$, then it satisfies the ℓ_1 robust null space property for S with constants $0 < \rho < 1, \tau' := \tau\sqrt{s} > 0$.*

Proof. For any $v \in \mathbb{C}^N$, $\|v_S\|_2 \leq \frac{\rho}{\sqrt{s}}\|v_{\bar{S}}\|_1 + \tau\|Av\|$. Then, using the fact that $\|v_S\|_1 \leq \sqrt{s}\|v_S\|_2$, we get: $\|v_S\|_1 \leq \rho\|v_{\bar{S}}\|_1 + \tau\sqrt{s}\|Av\|$. \square

Lemma 15 (Theorem 4.20 in [8]). *If a matrix $A \in \mathbb{C}^{m \times N}$ satisfies the ℓ_1 robust null space property (with respect to $\|\cdot\|$) and for $0 < \rho < 1$ and $\tau > 0$ for $S \subset [N]$, then:*

$$\|z - x\|_1 \leq \frac{1+\rho}{1-\rho}(\|z\|_1 - \|x\|_1 + 2\|x_{\bar{S}}\|_1) + \frac{2\tau}{1-\rho}\|A(z-x)\|$$

for all $z, x \in \mathbb{C}^N$.

Lemma 16 (Proposition 2.3 in [8]). *For any $p > q > 0$ and $x \in \mathbb{C}^n$,*

$$\inf_{z \in M_k} \|x - z\|_p \leq \frac{1}{(k)^{\frac{1}{q} - \frac{1}{p}}} \|x\|_q$$

Proof of Theorem 3. Let $0 < \rho < 1$ be arbitrary. Since F is a unitary matrix, for any $S \subseteq [n]$ and $v \in \mathbb{C}^n$, we have

$$\|v_S\|_2 \leq \frac{\rho}{\sqrt{k}}\|v_{\bar{S}}\|_1 + \tau\|v\|_2 = \frac{\rho}{\sqrt{k}}\|v_{\bar{S}}\|_1 + \tau\|Fv\|_2 \quad (15)$$

where $\tau = 1$. Therefore, F satisfies the ℓ_2 robust null space property for all $S \subseteq [n]$ with $\text{card}(S) \leq k$. Next, using Lemma 14 we get $\|v_S\|_1 \leq \rho\|v_{\bar{S}}\|_1 + \tau\sqrt{k}\|Fv\|_2$ for all $v \in \mathbb{C}^n$. Now let $x^\# =$

BP(y, F, η), then we know $\|x^\# \|_1 \leq \|x\|_1$, where x is k -sparse. Then letting $S \subseteq [n]$ be the support of x and using the fact that $\|x_{\bar{S}}\|_2 = 0$ and Lemma 15, we get:

$$\begin{aligned} \|x^\# - x\|_1 &\leq \frac{1+\rho}{1-\rho}(\|x^\# \|_1 - \|x\|_1 + 2\|x_{\bar{S}}\|_1) + \frac{2\tau\sqrt{k}}{1-\rho}\|F(x^\# - x)\|_2 \\ &\leq \frac{2\tau\sqrt{k}}{1-\rho}\|F(x^\# - x)\|_2 \leq \frac{4\tau\sqrt{k}}{1-\rho}\|e\|_2 \leq \frac{4\tau\sqrt{k}}{1-\rho}\eta \end{aligned}$$

Letting $\rho \rightarrow 0$ and recalling that $\tau = 1$ gives (6). Now let S be the support of the k largest entries in $x^\# - x$. Note $\|(x^\# - x)_{\bar{S}}\|_2 = \inf_{z \in M_k} \|(x^\# - x) - z\|_2$. Then, using Lemma 16 and (15), we see that

$$\begin{aligned} \|x^\# - x\|_2 &\leq \|(x^\# - x)_{\bar{S}}\|_2 + \|(x^\# - x)_S\|_2 \\ &\leq \frac{1}{\sqrt{k}}\|(x^\# - x)\|_1 + \frac{\rho}{\sqrt{k}}\|(x^\# - x)_{\bar{S}}\|_1 + \tau\|F(x^\# - x)\|_2 \\ &\leq \frac{1+\rho}{\sqrt{k}}\|(x^\# - x)\|_1 + 2\tau\eta \leq \frac{4\tau(1+\rho)}{(1-\rho)}\eta + 2\tau\eta = \left(\frac{4\tau(1+\rho)}{(1-\rho)} + 2\tau\right)\eta \end{aligned}$$

Recalling $\tau = 1$ and letting $\rho \rightarrow 0$ gives the desired result. \square

7 Dantzig Selector

Next we introduce the Dantzig Selector algorithm with an additional constraint. We first prove its recovery guarantees for ℓ_∞ -norm and then explain the reasoning behind the additional constraint.

Algorithm 3 Modified Dantzig Selector

Input: The observed vector $y \in \mathbb{C}^m$, where $y = A\hat{x} + e$, the measurement matrix $A \in \mathbb{C}^{m \times N}$, and constants η_1, η_2 such that $\|e\|_\infty \leq \eta_1, \|A^*e\|_\infty \leq \eta_2$

Output: $x^\# \in \mathbb{C}^N$

- 1: **procedure** DS(y, A, η_1, η_2)
 - 2: $x^\# \leftarrow \arg \min_{z \in \mathbb{C}^N} \|z\|_1$ subject to $\|A^*(y - Az)\|_\infty \leq \eta_2, \|Az - y\|_\infty \leq \eta_1$
 - 3: **return** $x^\#$
-

Proof of Theorem 4. The proof follows the same structure as the proof of Theorem 3. Therefore we provide a sketch and leave out the complete derivation. Let $0 < \rho < 1$ be arbitrary. Since F is a unitary matrix, for any $S \subseteq [n]$ and $v \in \mathbb{C}^n$, we have

$$\|v_S\|_2 \leq \frac{\rho}{\sqrt{k}}\|v_{\bar{S}}\|_1 + \|v_S\|_2 \leq \frac{\rho}{\sqrt{k}}\|v_{\bar{S}}\|_1 + \sqrt{k}\|v\|_\infty = \frac{\rho}{\sqrt{k}}\|v_{\bar{S}}\|_1 + \sqrt{k}\|F^*Fv\|_\infty$$

The rest of the argument is the same as in the proof of Theorem 3. \square

7.1 Additional Constraint on DS

We now comment on the additional constraint $\|Az - y\|_\infty \leq \eta_1$ in the statement of Algorithm 3. Observe that the constraint is: $|(Az)_i - (A\hat{x})_i - e_i| \leq \eta_1$ for any $i \in [n]$. Since $\|e\|_\infty \leq \eta_1$, the constraint implies $|(Az)_i - (A\hat{x})_i| \leq 2\eta_1$. Now suppose that our input is an image $x = F^*\hat{x}$,

Layer	Type	Properties
1	Convolution	32 channels, 3×3 Kernel, No padding
2	Convolution	64 channels, 3×3 Kernel, No padding, Dropout with $p = 0.5$
3	Max-pooling	2×2 , Dropout with $p = 0.5$
4	Fully Connected	128 neurons, Dropout with $p = 0.5$
5	Fully Connected	10 neurons

Table 1: Network architecture used for MNIST and Fashion-MNIST datasets in Section 8.2 and Section 8.3. The first four layers use ReLU activations while the last layer uses a softmax activation.

Dataset	t_{avg}	δ_{ℓ_∞}	δ_{ℓ_2}	Δ_{ℓ_∞}	Δ_{ℓ_2}
CIFAR-10	1.52	0.19	0.27	5.38	17.34
MNIST	1.47	0.14	0.19	3.46	9.99
Fashion-MNIST	1.50	0.10	0.14	2.87	8.27

Table 2: Recovery performance of Algorithm 1 on ℓ_0 -norm bounded noise.

where F is the Discrete Fourier Transform matrix. Setting $A = F^*$, the constraint ensures that the entries of a reconstructed image F^*z and the original image $F^*\hat{x}$ will be close. That is, the constraint limits the feasible set of solutions to those that will lead to better reconstruction quality. This is particularly useful when we need to utilize the reconstructed images for some downstream task such as classification by a neural network. On the other hand suppose that we do not add this constraint. Then, since $\|F^*e\|_\infty \leq \sqrt{n}\eta_1$ grows with the dimension of the ambient space, there is no guarantee that the reconstruction will be close to the original image, especially when $\sqrt{n}\eta_1$ is large.

8 Experiments

We first analyze how our recovery guarantees perform in practice (Section 8.1) and then show that CRD can be used to defend neural networks against ℓ_0 -norm attacks (Section 8.2), ℓ_2 -norm attacks (Section 8.1.2) as well as ℓ_∞ -norm attacks (Section 8.1.3).

All of our experiments are conducted on CIFAR-10 [13], MNIST [15], and Fashion-MNIST [29] datasets with pixel values of each image normalized to lie in $[0, 1]$. For every experiment, we use the Discrete Cosine Transform (DCT) and the Inverse Discrete Cosine Transform (IDCT) denoted by the matrices $F \in \mathbb{R}^{n \times n}$ and $F^T \in \mathbb{R}^{n \times n}$ respectively. That is, for an adversarial image $y \in \mathbb{R}^{\sqrt{n} \times \sqrt{n}}$, such that, $y = x + e$, we let $\hat{x} = Fx$, and $x = F^T\hat{x}$, where $x, \hat{x} \in \mathbb{R}^n$ and $e \in \mathbb{R}^n$ is the noise vector. For an adversarial image $y \in \mathbb{R}^{\sqrt{n} \times \sqrt{n} \times c}$, that contains c channels, we perform recovery on each channel independently by considering $y_m = x_m + e_m$, where $\hat{x}_m = Fx_m$, $x_m = F^T\hat{x}_m$ for $m = 1, \dots, c$. The value k denotes the number of largest (in absolute value) DCT co-efficients used for reconstruction of each channel, and the value t denotes the ℓ_0 noise budget for each channel.

We now outline the neural network architectures used for experiments in Section 8.2 and 8.3. For CIFAR-10, we use the network architecture of [10] while the network architecture for MNIST and Fashion-MNIST datasets is provided in Table 1. We train our networks using the Adam optimizer for CIFAR-10 and the AdaDelta optimizer for MNIST and Fashion-MNIST. In both cases, we use a cross-entropy loss function. We implement the following training procedure: for every training image x , we first generate $\hat{x}_{h(k)} = (Fx)_{h(k)}$, and then reconstruct the image $x' = F^T\hat{x}_{h(k)}$. We then

Dataset	t_{avg}	δ_{ℓ_2}	Δ_{ℓ_2}
CIFAR-10	4.03	20.10	866.07
MNIST	4.01	5.08	381.33
Fashion-MNIST	4.02	6.84	298.73

Table 3: Recovery performance of Algorithm 2 for ℓ_0 -norm bounded noise.

Dataset	$\ell_{2\text{avg}}$	δ_{ℓ_1}	δ_{ℓ_2}	Δ_{ℓ_1}	Δ_{ℓ_2}
CIFAR-10	32.03	88.56	17.45	2015.47	315.22
MNIST	16.15	43.87	8.20	365.17	88.80
Fashion-MNIST	16.16	40.90	9.32	367.94	87.64

Table 4: Recovery performance of Algorithm 2 for ℓ_2 -norm bounded noise.

use both x and x' to train the network. For instance, in MNIST we get 60000 original training images and 60000 reconstructed training images, for a total of 120000 training images. The code to reproduce our experiments is available here: https://github.com/jasjeetIM/recovering_compressible_signals.

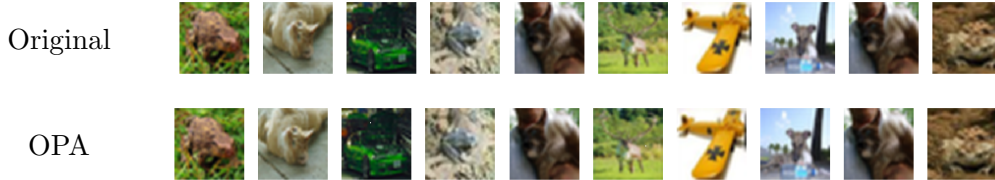


Figure 1: Adversarial images for CIFAR-10 created using OPA. The original images are shown in the first row, and the adversarial images are shown in the second row.

8.1 Recovery Error

Since recovery guarantees have been proved theoretically, our aim is to examine how close the recovery error is to the upper bound in practice. Each experiment is conducted on a subset of 500 data points sampled uniformly at random from the respective dataset. The first metric we report is $\delta_{\ell_p} := \frac{1}{500} \sum_{i=1}^{500} \|x_i^\# - (\hat{x}_i)_{h(k)}\|_p$, where $x_i^\#$ is the recovered vector for the noisy measurement y_i , $(\hat{x}_i)_{h(k)} = (Fx_i)_{h(k)}$ and the average is taken over the 500 points sampled from the dataset. This measures the average magnitude of the recovery error for the respective algorithm in ℓ_p norm. In order to relate this value to the upper bound on the recovery error, we also report $\Delta_{\ell_p} := \frac{1}{500} \sum_{i=1}^{500} (\Upsilon_i - \|x_i^\# - (\hat{x}_i)_{h(k)}\|_p)$, where Υ_i is the guaranteed upper bound for y_i . Using δ_{ℓ_p} and Δ_{ℓ_p} , we aim to capture how much smaller the recovery error is than the upper bound for these datasets.

8.1.1 ℓ_0 noise

For each data point $x_i \in \mathbb{R}^n, i = 1, 2, \dots, 500$, we construct a noise vector $e_i \in \mathbb{R}^n$ as follows: we first sample an integer t_i from a uniform distribution over the set $\{1, \dots, t\}$, where t is the allowed ℓ_0

Dataset	$\ell_{\infty\text{avg}}$	δ_{ℓ_1}	δ_{ℓ_2}	Δ_{ℓ_1}	Δ_{ℓ_2}
CIFAR-10	0.99	10821.49	1435.45	4538.50	2207.48
MNIST	0.99	1519.27	213.23	2960.72	849.28
Fashion-MNIST	0.99	1824.30	274.21	2655.69	788.30

Table 5: Recovery performance of Algorithm 3 for ℓ_{∞} -norm bounded noise.

Orig. Acc.	OPA. Acc	IHT. Acc.
77.4%	0.0%	71.8%

Table 6: Effectiveness of CRD against OPA. The first column lists the accuracy of the network on original images and the OPA Acc. columns shows the network’s accuracy on adversarial images. The IHT. Acc. column shows the accuracy of the network on images reconstructed using Algorithm 1.

noise budget. Next, we select an index set $S_{t_i} \subset [n]$ uniformly at random, such that $\text{card}(S_{t_i}) = t_i$. Then for each $j \in S_{t_i}$, we set $(e_i)_j = c_j$, where c_j is sampled from the uniform distribution on $[0, 1)$ and $(e_i)_l = 0$ for $l \notin S_{t_i}$. We then set $y_i = x_i + e_i$ as the observed noisy vector. We report $\delta_{\ell_{\infty}}, \delta_{\ell_2}, \Delta_{\ell_{\infty}}, \Delta_{\ell_2}$ and $t_{\text{avg}} := \frac{1}{500} \sum_{i=1}^{500} t_i$.

Recovery with Algorithm 1

We examine how (13) and (14) perform in practice. To do so, we set $k = 4$ for MNIST and Fashion-MNIST and are allowed an ℓ_0 noise budget of $t = 3$. For CIFAR-10, we set $k = 5$ and are allowed a noise budget of $t = 3$. We note that k values have been chosen to meet our computational constraints. As such, any other values that fit the hypotheses of (13) and (14) would work just as well. The results in Table 2 show that on average, the recovery error is well below the upper bounds.

Recovery with Algorithm 2

We implement Algorithm 2 using the open source library CVXPY [6]. We set $k = 8$ for MNIST and Fashion-MNIST and are allowed an ℓ_0 noise budget of $t = 8$. For CIFAR-10, we set $k = 10$ and are allowed a noise budget of $t = 8$. We observe the results in Table 3 and note once again that the recovery error is well below the upper bound of (5).

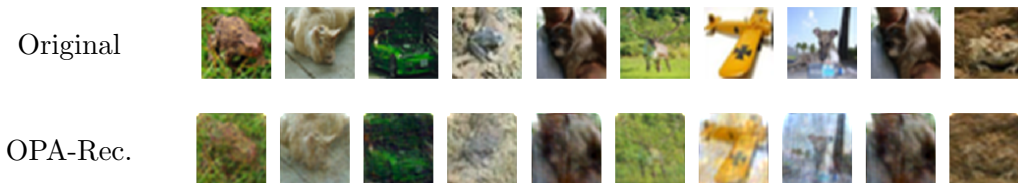


Figure 2: Reconstruction quality of images using Algorithm 1. The first row shows the original images while the second row shows reconstruction from the largest 275 DCT co-efficients recovered using Algorithm 1.

8.1.2 ℓ_2 noise

Now we consider the case when the noise vector $e_i, i = 1, 2, \dots, 500$ is only bounded in ℓ_2 -norm. For each $e_i, i = 1, 2, \dots, 500$, we set $(e_i)_j = c_j$, where c_j is sampled from the uniform distribution on $[0, 1)$. Since there is no restriction on how small k needs to be, we set $k = 75$ for CIFAR-10 and $k = 40$ for MNIST and Fashion-MNIST. We report $\delta_{\ell_1}, \delta_{\ell_2}, \Delta_{\ell_1}, \Delta_{\ell_2}$ and since the noise budget is in ℓ_2 -norm, we also report $\ell_{2_{\text{avg}}} := \sum_{i=1}^{500} \|e_i\|_2$. The results are shown in Table 4. As was the case in the Section 8.1.1, the recovery error is well below the upper bounds of (6) and (7).

8.1.3 ℓ_∞ noise

We follow the same procedure as in Section 8.1.2 to construct noise vectors $e_i, i = 1, 2, \dots, 500$. This ensures that $\|e\|_\infty \leq 1$. We also select the value of k as done in Section 8.1.2 as well. We report $\delta_{\ell_1}, \delta_{\ell_2}, \Delta_{\ell_1}, \Delta_{\ell_2}$ as well as $\ell_{\infty_{\text{avg}}} := \sum_{i=1}^{500} \|e_i\|_\infty$. Once again recovery error is well below the upper bounds of (8) and (9) as shown in Table 5.

8.2 Defense against ℓ_0 -norm attacks

This section is organized as follows: first we examine CRD against the One Pixel Attack (OPA) [23] for CIFAR-10. We only test the attack on CIFAR-10 as it is most effective against natural images and does not work well on MNIST or FASHION-MNIST. We note that this attack satisfies the theoretical constraints for t provided (13) and (14), hence allowing us to test how well CRD works within existing guarantees. Once we establish the effectiveness of CRD against OPA, we then test it against two other ℓ_0 -norm bounded attacks: Carlini and Wagner (CW) ℓ_0 -norm attack [4] and the Jacobian based Saliency Map Attack (JSMA) [20]. Each experiment is conducted on a set of 1000 points sampled uniformly at random from the test set of the respective dataset.

8.2.1 One Pixel Attack

We first resize all CIFAR-10 images to $125 \times 125 \times 3$ while maintaining aspect ratios to ensure that the data falls under the hypotheses of (13) and (14) even for large values of k . The OPA attack perturbs exactly one pixel of the image, leading to an ℓ_0 noise budget of $t = 3$ per image. The ℓ_0 noise budget of $t = 3$ per image allows us to use $k = 275$ per channel. Table 6 shows that OPA is very effective against natural images and forces the network to misclassify all previously correctly classified inputs. Figure 1 shows that adversarial images created using OPA are visually almost indistinguishable from the original images. We test the performance of CRD in two ways: a) reconstruction quality b) network performance on reconstructed images.

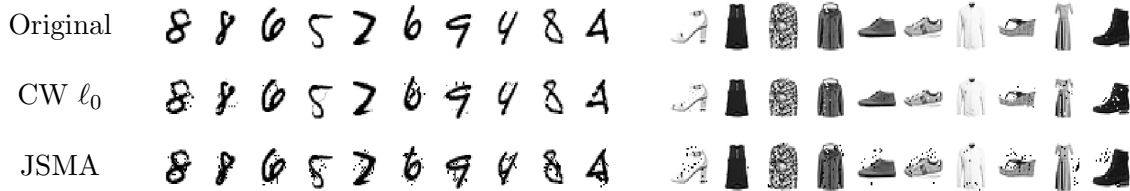


Figure 3: Adversarial images for MNIST and Fashion-MNIST datasets for ℓ_0 -norm bounded attacks. The first row lists the original images, while the second row shows adversarial images created using the CW ℓ_0 -norm attack and the third row shows adversarial images created using the JSMA attack.

In order to analyse the reconstruction quality of Algorithm 1, we do the following: for each test image, we use OPA to perturb the image and then use Algorithm 1 to approximate its largest (in absolute value) $k = 275$ DCT co-efficients. We then perform the IDCT on these recovered co-efficients to generate reconstructed images. The reconstructed images from Algorithm 1 can be seen in the second row of Figure 2.

Noting that Algorithm 1 leads to high quality reconstruction, we now test whether network accuracy improves on these reconstructed images. To do so, we feed these reconstructed images as input to the network and report its accuracy in Table 6. We note that network performance does indeed improve as network accuracy goes from 0.0% to 71.8% using Algorithm 1. Therefore, we conclude that CRD provides a substantial improvement in accuracy in against OPA.

8.2.2 CW- ℓ_0 Attack and JSMA

Having established the effectiveness of CRD against OPA, we move onto the CW ℓ_0 -norm attack and JSMA. We note that even when t is much larger than the hypotheses of Theorem 1 and Theorem 2, we find that Algorithms 1 and 2 are still able to defend the network. We hypothesize that this maybe related to the behavior of the RIP of a matrix for “most”² vectors as opposed to the RIP for all vectors, and leave a more rigorous analysis for a follow up work.

To begin our analysis, we show adversarial images for MNIST and Fashion-MNIST created by CW- ℓ_0 and JSMA in Figure 3. The first row contains the original test images while the second and the third rows show the adversarial images. We show adversarial images for the CIFAR-10 dataset in Figure 4.

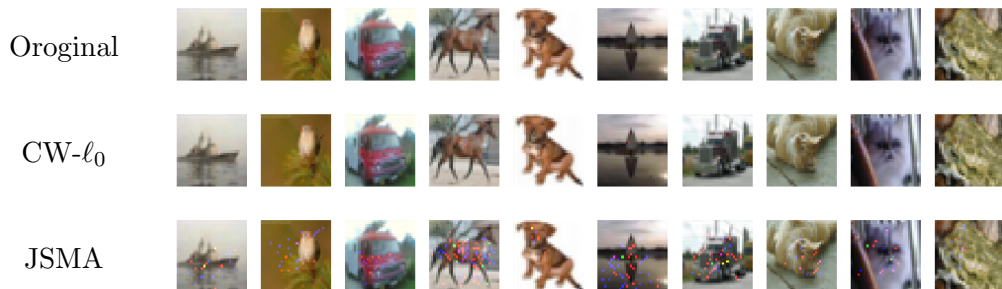


Figure 4: Adversarial images for the CIFAR-10 dataset showing ℓ_0 -norm attacks. The first row contains the original images, the second row shows images created using the CW ℓ_0 -norm attack and the third row shows images created using the JSMA attack.

Next, we follow the procedure described in Section 8.2.1 to analyze the quality of reconstructions for Algorithm 1 and Algorithm 2. For MNIST and Fashion-MNIST, we show the reconstructions of Algorithm 1 in Figure 5 and for Algorithm 2 in Figure 6. For CIFAR-10, we show the reconstructions for Algorithm 1 in Figure 7 and for Algorithm 2 in Figure 8. In each case it can be seen that both algorithms provide high quality reconstructions for values of t that are well outside the hypotheses required by Theorem 1 and Theorem 2. We report these t values and the improvement in network performance on reconstructed adversarial images using CRD in Table 7.

²Recall that the results of Theorems 1 and 2 hold for all vectors in \mathbb{C}^n , while for the vectors we considered (CIFAR-10, MNIST, Fashion-MNIST), the recovery error in Section 8.1.1 was well below the guarantees.

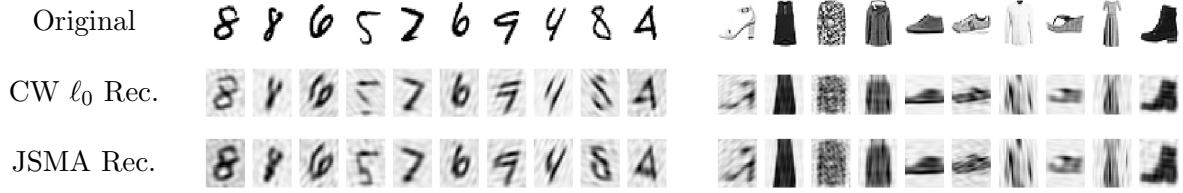


Figure 5: Reconstruction from adversarial images using Algorithm 1. The first row shows the original images while the second and third rows show the reconstruction of the adversarial images after recovering the largest 40 co-efficients using Algorithm 1.

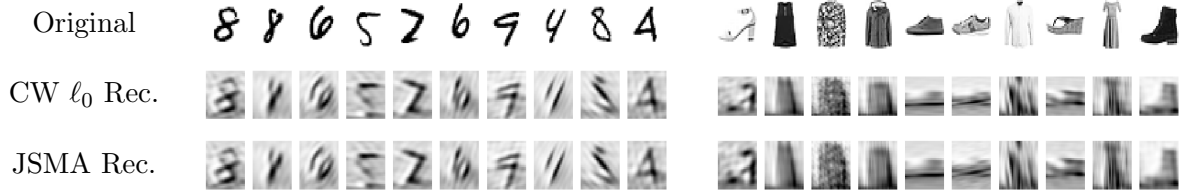


Figure 6: Reconstruction quality of Algorithm 2. The first row shows the original images while the second and third rows show the reconstruction of the adversarial images after recovering the largest 40 co-efficients using Algorithm 2.

8.3 Defense against ℓ_2 -norm attacks

In the case of ℓ_2 -norm bounded attacks, we use the CW ℓ_2 -norm attack [4] and the Deepfool attack [19] as they have been shown to be the most powerful. We note that Theorem 3 does not impose any restrictions on k or t and therefore the guarantees of equations (6) and (7) are applicable for recovery in all experiments of this section. Figure 9 shows examples of each attack for the CIFAR-10 dataset while adversarial images for MNIST and Fashion-MNIST are presented in Figure 10.

The reconstruction quality for MNIST and Fashion-MNIST is shown in Figure 11 and for CIFAR-10 we show the reconstruction quality in Figure 12. It can be noted that reconstruction using Algorithm 2 is of high quality for all three datasets. In order to check whether this high quality

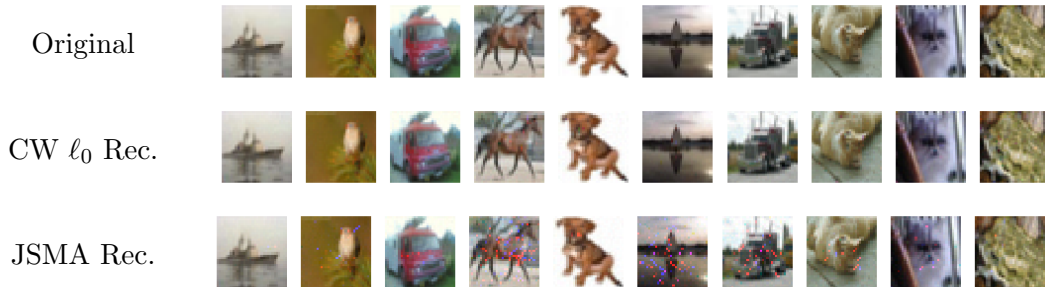


Figure 7: Reconstruction quality of Algorithm 1 for CIFAR-10. The first row shows the original images while the second and the third rows show reconstructions of the CW- ℓ_0 and JSMA adversarial images after recovering the largest 500 co-efficients via Algorithm 1

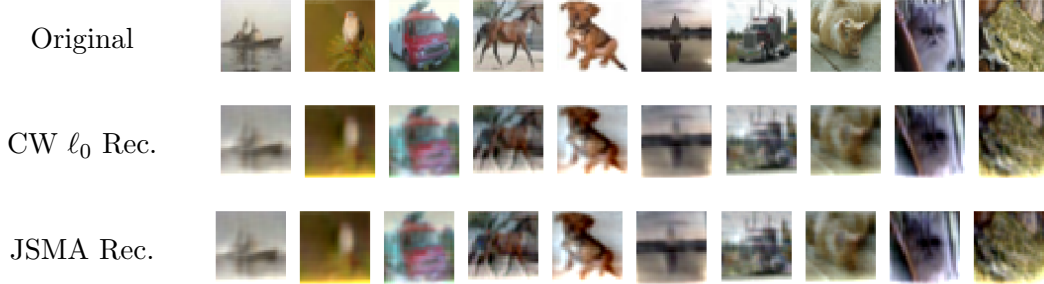


Figure 8: Reconstruction quality of Algorithm 2 on CIFAR-10. The first row shows the original images while the second and the third rows show reconstructions of the CW- ℓ_0 and JSMA adversarial images after recovering all 1024 co-efficients using Algorithm 2.

Dataset	Orig.	C&W ℓ_0				JSMA			
	Acc.	t_{avg}	Acc.	IHT Acc.	BP Acc.	t_{avg}	Acc.	IHT Acc.	BP Acc.
CIFAR-10	84.9%	18	8.7%	83.0%	67.0%	34	2.7%	63.2%	67.3%
MNIST	98.8%	15	0.9%	84.2%	55.9%	17	56.5 %	90.1%	67.4%
F-MNIST	91.8%	16	5.27%	84.1%	71.4%	17	62.6 %	83.3%	72.0%

Table 7: Network performance on the original inputs, adversarial inputs and the inputs corrected using CRD. Here the t_{avg} column lists the average adversarial budget for each attack, Orig. Acc. column lists the accuracy of the network on the original inputs, the Acc. columns shows the accuracy on adversarial inputs, the IHT Acc. and the BP Acc. columns list the accuracy of the network on inputs that have been corrected using Algorithm 1 and Algorithm 2 respectively.

reconstruction also leads to improved performance in network accuracy, we test each network on reconstructed images using Algorithm 2. We report the results in Table 8 and note that Algorithm 2 provides a substantial improvement in network accuracy for each dataset and each attack method used.

8.4 Defense against ℓ_∞ -norm attacks

For ℓ_∞ -norm bounded attacks, we use the BIM attack [14] as it has been shown to be very effective and also allows one to control the ℓ_∞ -norm of the attack vector explicitly. We note that while the CW ℓ_∞ -norm attack [4] has the ability to create attack vectors with ℓ_∞ -norm less than or equal to BIM, it is computationally expensive and also does not allow one to pre-specify a value for the ℓ_∞ -norm of an attack vector. Therefore, we limit our experimental analysis to the BIM attack. Note that for any attack vector e , $\|e\|_2 \leq \sqrt{n}\|e\|_\infty$ hence allowing ℓ_∞ -norm attacks to create attack vectors with large ℓ_2 -norm. Therefore, we could expect reconstruction quality and network accuracy to be lower when compared to ℓ_2 -norm attacks. Figure 13 shows examples of each attack for the MNIST and Fashion-MNIST datasets while images for CIFAR-10 are presented in Figure 14. We show reconstructions using Algorithm 3 in Figures 15 and 16. Finally, we report the network performance on reconstructed inputs using Algorithm 3 in Table 9. We note that Algorithm 3 provides an increase in network performance against reconstructed adversarial inputs. However, the improvement in performance is not as substantial as it was against ℓ_0 or ℓ_2 -norm attacks.

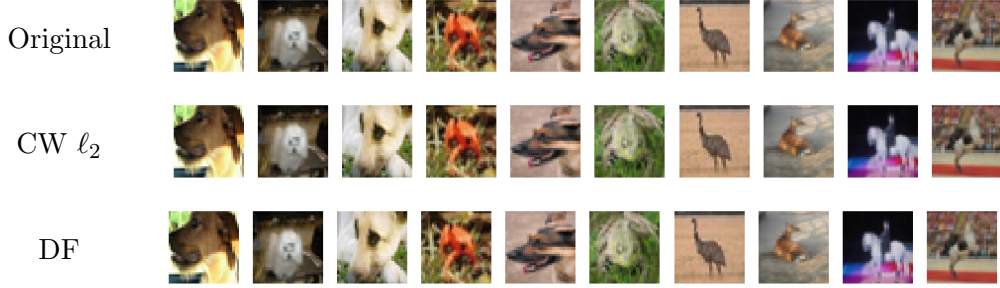


Figure 9: Adversarial images for the CIFAR-10 dataset showing ℓ_2 -norm attacks. The first row contains the original images, the second row shows images created using the CW ℓ_2 -norm attack and the third row shows images created using the DeepFool attack.

Dataset	Orig.	C&W ℓ_2			Deepfool		
	Acc.	$\ell_{2\text{avg}}$	Acc.	BP Acc.	$\ell_{2\text{avg}}$	Acc.	BP Acc.
CIFAR-10	84.9%	0.12	8.7%	72.3%	0.11	7.7%	71.6%
MNIST	99.17%	1.35	0.9%	92.4%	1.72	1.1 %	90.7%
Fashion-MNIST	90.3%	0.61	5.4%	78.3%	0.63	5.5 %	76.4%

Table 8: Accuracy of our network on the original inputs, adversarial inputs and the inputs corrected using CRD. Here the $\ell_{2\text{avg}}$ column lists the average ℓ_2 -norm of the attack vector, Acc. columns list the accuracy of the network on the original and adversarial inputs, and the BP Acc. columns lists the accuracy of the network on inputs reconstructed using Algorithm 2.

8.5 Which recovery algorithm to use for ℓ_0 -norm attacks

As shown in Section 8.1.1, Algorithm 1 and Algorithm 2 lead to high quality reconstructions for ℓ_0 -norm bounded attacks. Hence, it is conceivable that CRD using either algorithm should be able to provide a good defense. However, we note that the ℓ_2 -norm recovery error is lower for Algorithm 1 as seen in Section 8.1.1. Therefore, depending on the dataset, Algorithm 1 may lead to better quality reconstructions and hence better network accuracy. From a practical perspective, one may ask which algorithm is faster. Since Algorithm 2 is not technically an algorithm, its runtime is dependent on the actual method used to solve the optimization problem. For instance, we use Second Order Cone Programming (SOCP) from CVXPY [6] for solving the minimization problem

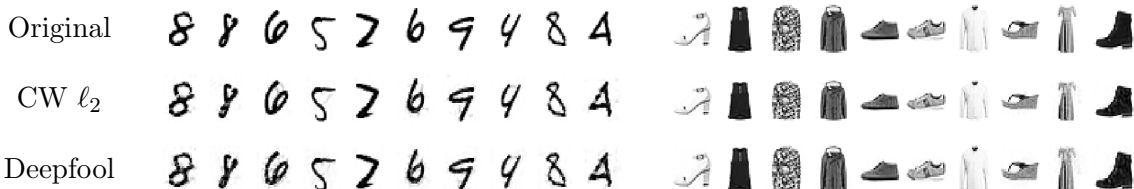


Figure 10: Adversarial images for MNIST and Fashion-MNIST datasets for ℓ_2 -norm bounded attacks. The first row lists the original images for the MNIST and Fashion MNIST dataset. The second row shows adversarial images created using the CW ℓ_2 -norm attack and the third row shows adversarial images created using the Deepfool attack.

Dataset	Orig. Acc.	BIM		
		$\ell_{\infty \text{avg}}$	Acc.	DS Acc.
CIFAR-10	84.9%	0.015	7.4%	49.4%
MNIST	99.17%	0.15	4.9%	74.7%
Fashion-MNIST	90.3%	0.15	5.3%	57.5%

Table 9: Defense against ℓ_{∞} attacks using CRD. Here $\ell_{\infty \text{avg}}$ column lists the ℓ_{∞} -norm of each attack vector, Acc. columns list the accuracy of the network on the original and adversarial inputs, and the DS Acc. columns lists the accuracy of the network on inputs reconstructed using Algorithm 3.

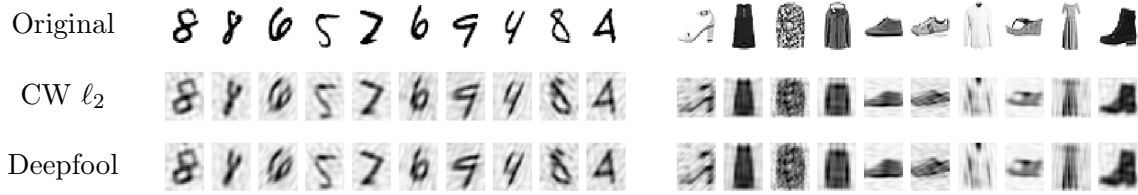


Figure 11: Reconstruction from adversarial images using Algorithm 2. The first row shows the original images while the second and the third rows show the reconstruction of the adversarial images after recovering the largest 40 co-efficients using Algorithm 2.

in Algorithm 2. In our experiments, we noticed that the runtime of Algorithm 2 slows considerably for larger values of n . However, Algorithm 1 does not face this issue (there is a slowdown but it is much smaller than Algorithm 2). Therefore, if speed is important, it may be beneficial to use Algorithm 1 as opposed to Algorithm 2.

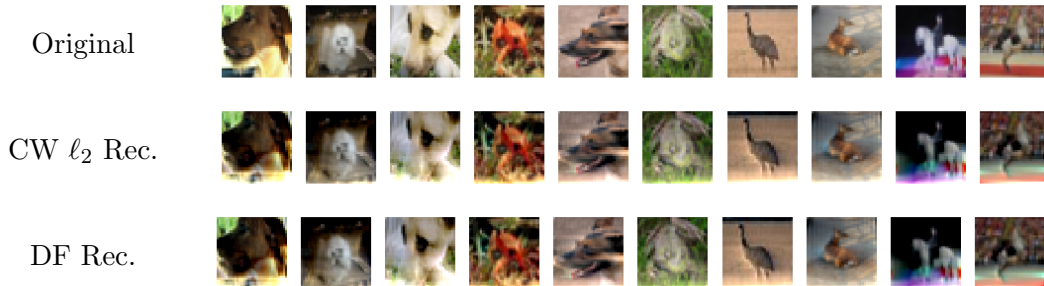


Figure 12: Reconstruction quality of Algorithm 2. The first row shows the original images, the second row shows reconstruction of CW- ℓ_2 and DeepFool images using 1024 co-efficients recovered via Algorithm 2.

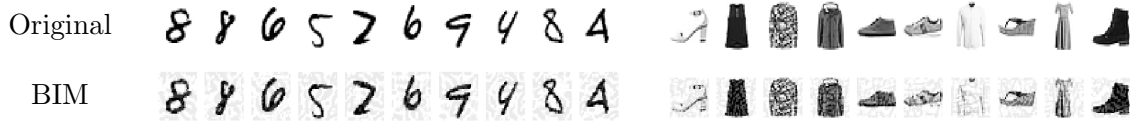


Figure 13: Adversarial images for MNIST and Fashion-MNIST datasets for ℓ_∞ -norm bounded attacks. The first row lists the original images, while the second row shows adversarial images created using the BIM attack.

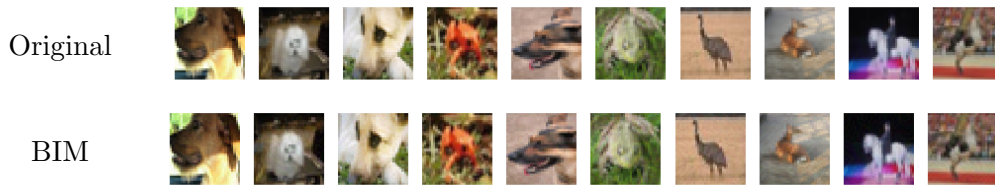


Figure 14: Adversarial images for the CIFAR-10 dataset showing the BIM attack. The first row contains the original images, the second row shows images created using the BIM attack.



Figure 15: Reconstruction from adversarial images using Algorithm 3. The first row shows the original images while the second and the third rows show the reconstruction of the adversarial images after recovering the largest 40 co-efficients using Algorithm 3.

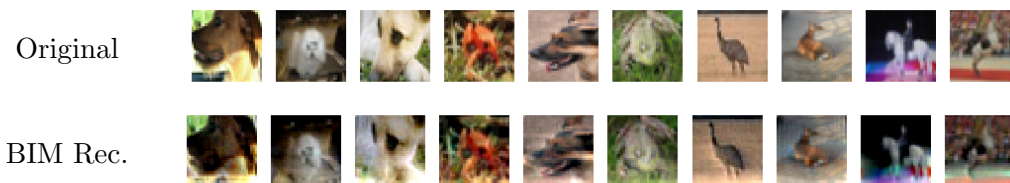


Figure 16: Reconstruction quality of Algorithm 3. The first row shows the original images, the second row shows reconstruction of BIM images using 1024 co-efficients recovered via Algorithm 3.

9 Conclusion

We provided recovery guarantees for corrupted signals in the case of ℓ_0 -norm, ℓ_2 -norm, and ℓ_∞ -norm bounded noise. We then experimentally verified these guarantees and showed that for the datasets used, recovery error was considerably lower than the upper bounds of our theorems. We were able to utilize these observations in CRD and improve the performance of neural networks substantially in the case of ℓ_0 -norm, ℓ_2 -norm and ℓ_∞ -norm bounded noise. While ℓ_0 -norm attacks don't necessarily satisfy the constraints required by Theorem 1 and Theorem 2, we showed that CRD is still able to provide a good defense for values of t much larger than allowed in the guarantees. The guarantees of Theorem 3 and Theorem 4 were applicable in all experiments and CRD was shown to improve network performance for all attacks.

References

- [1] Mitali Bafna, Jack Murtagh, and Nikhil Vyas. Thwarting adversarial examples: An l_0 -robust sparse fourier transform. In *Advances in Neural Information Processing Systems*, pages 10075–10085, 2018.
- [2] Richard G. Baraniuk, Volkan Cevher, Marco F. Duarte, and Chinmay Hedge. Model-based compressive sensing. *IEEE Transactions on Information Theory*, 56(4):1982–2001, 2010.
- [3] Emmanuel J Candes, Justin K Romberg, and Terence Tao. Stable signal recovery from incomplete and inaccurate measurements. *Communications on Pure and Applied Mathematics: A Journal Issued by the Courant Institute of Mathematical Sciences*, 59(8):1207–1223, 2006.
- [4] Nicholas Carlini and David Wagner. Towards evaluating the robustness of neural networks. In *2017 IEEE Symposium on Security and Privacy (SP)*, pages 39–57. IEEE, 2017.
- [5] Moustapha Cisse, Piotr Bojanowski, Edouard Grave, Yann Dauphin, and Nicolas Usunier. Parseval networks: Improving robustness to adversarial examples. In *Proceedings of the 34th International Conference on Machine Learning-Volume 70*, pages 854–863. JMLR. org, 2017.
- [6] Steven Diamond and Stephen Boyd. CVXPY: A Python-embedded modeling language for convex optimization. *Journal of Machine Learning Research*, 17(83):1–5, 2016.
- [7] Cynthia Dwork, Aaron Roth, et al. The algorithmic foundations of differential privacy. *Foundations and Trends® in Theoretical Computer Science*, 9(3–4):211–407, 2014.
- [8] Simon Foucart and Holger Rauhut. *A Mathematical Introduction to Compressive Sensing*. 2017.
- [9] I.J. Goodfellow, J. Shlens, and C. Szegedy. Explaining and harnessing adversarial examples. In *International Conference on Learning Representations*, 2015.
- [10] Kaiming He, Xiangyu Zhang, Shaoqing Ren, and Jian Sun. Deep residual learning for image recognition. In *Proceedings of the IEEE conference on computer vision and pattern recognition*, pages 770–778, 2016.
- [11] M. Hein and M. Andriushchenko. Formal guarantees on the robustness of a classifier against adversarial manipulation. In *Advances in Neural Information Processing Systems 30: Annual Conference on Neural Information Processing Systems 2017, 4-9 December 2017, Long Beach, CA, USA*, pages 2263–2273, 2017.
- [12] A. Krizhevsky, I. Sutskever, and G. E Hinton. Imagenet classification with deep convolutional neural networks. In *Advances in neural information processing systems*, pages 1097–1105, 2012.
- [13] Alex Krizhevsky. Learning multiple layers of features from tiny images. Technical report, Citeseer, 2009.
- [14] Alexey Kurakin, Ian Goodfellow, and Samy Bengio. Adversarial examples in the physical world. *arXiv preprint arXiv:1607.02533*, 2016.
- [15] Yann LeCun. The mnist database of handwritten digits. <http://yann.lecun.com/exdb/mnist/>.

- [16] Mathias Lecuyer, Vaggelis Atlidakis, Roxana Geambasu, Daniel Hsu, and Suman Jana. Certified robustness to adversarial examples with differential privacy. *arXiv preprint arXiv:1802.03471*, 2018.
- [17] Bai Li, Changyou Chen, Wenlin Wang, and Lawrence Carin. Second-order adversarial attack and certifiable robustness. *arXiv preprint arXiv:1809.03113*, 2018.
- [18] Aleksander Madry, Aleksandar Makelov, Ludwig Schmidt, Dimitris Tsipras, and Adrian Vladu. Towards deep learning models resistant to adversarial attacks. *arXiv preprint arXiv:1706.06083*, 2017.
- [19] Seyed-Mohsen Moosavi-Dezfooli, Alhussein Fawzi, and Pascal Frossard. Deepfool: a simple and accurate method to fool deep neural networks. In *Proceedings of the IEEE conference on computer vision and pattern recognition*, pages 2574–2582, 2016.
- [20] Nicolas Papernot, Patrick McDaniel, Somesh Jha, Matt Fredrikson, Z Berkay Celik, and Ananthram Swami. The limitations of deep learning in adversarial settings. In *2016 IEEE European Symposium on Security and Privacy (EuroS&P)*, pages 372–387. IEEE, 2016.
- [21] Pouya Samangouei, Maya Kabkab, and Rama Chellappa. Defense-gan: Protecting classifiers against adversarial attacks using generative models. *arXiv preprint arXiv:1805.06605*, 2018.
- [22] Aman Sinha, Hongseok Namkoong, and John Duchi. Certifying some distributional robustness with principled adversarial training. *arXiv preprint arXiv:1710.10571*, 2017.
- [23] Jiawei Su, Danilo Vasconcellos Vargas, and Kouichi Sakurai. One pixel attack for fooling deep neural networks. *IEEE Transactions on Evolutionary Computation*, 2019.
- [24] I. Sutskever, O. Vinyals, and Q. V Le. Sequence to sequence learning with neural networks. In *Advances in neural information processing systems*, pages 3104–3112, 2014.
- [25] C. Szegedy, W. Zaremba, and I. Sutskever. Intriguing properties of neural networks. *International Conference on Learning Representations*, 2014.
- [26] Christian Szegedy, Wojciech Zaremba, Ilya Sutskever, Joan Bruna, Dumitru Erhan, Ian Goodfellow, and Rob Fergus. Intriguing properties of neural networks. *arXiv preprint arXiv:1312.6199*, 2013.
- [27] F. Tramèr, A. Kurakin, N. Papernot, D. Boneh, and P. McDaniel. Ensemble Adversarial Training: Attacks and Defenses. *ArXiv e-prints*, May 2017.
- [28] Eric Wong and J Zico Kolter. Provable defenses against adversarial examples via the convex outer adversarial polytope. *arXiv preprint arXiv:1711.00851*, 2017.
- [29] Han Xiao, Kashif Rasul, and Roland Vollgraf. Fashion-mnist: a novel image dataset for benchmarking machine learning algorithms. *arXiv preprint arXiv:1708.07747*, 2017.
- [30] W. Xu, D. Evans, and Y. Qi. Feature Squeezing Mitigates and Detects Carlini/Wagner Adversarial Examples. *ArXiv e-prints*, May 2017.